From adsorptation to dissipation: insights from computer simulations of solid H2O and CO

Ferrari, B.C.

Chapter 4

Abundance of Exceptionally Strong Binding Sites for H_2O Adsorption on the Ice Ih(0001) Surface

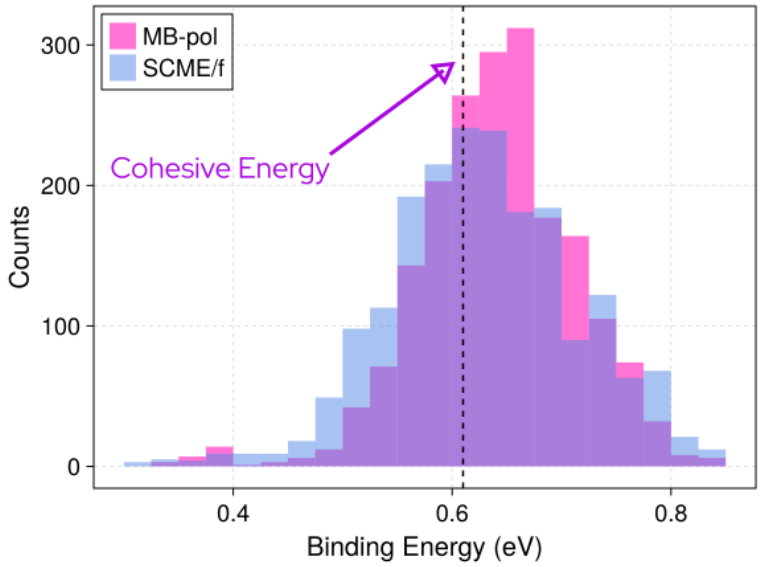

This chapter is based on:

Ferrari, B. C., Sallermann, M., Jónsson, E. O., Jónsson, H., & Meyer, J. (2026). Abundance of Exceptionally Strong Binding Sites for H_2O Adsorption on the Ice Ih(0001) Surface, *in prep.*

4.1 Abstract

The adsorption of water molecules on ice surfaces is of significant importance in many respects, in particular for gaining a deeper understanding of ice crystal growth. Due to the proton disorder on the ice Ih(0001) surface there is a wide distribution for the binding energy of admolecules. Previous calculations using simple point-charge force fields have indicated that it can even exceed the cohesive energy of the crystal at certain sites. While the accuracy of those calculations has been contested by some subsequent density functional theory calculations and direct measurement of these binding energy remains elusive, the possibility of such strong binding sites has been associated with various experimental observations and would significantly influence the growth mode of the crystal. Here, we study the adsorption of a water molecule on the ice Ih(0001) surface using recently developed polarizable many-body interaction potential functions, and find remarkably abundant sites with binding energy larger than the cohesive energy, dominated by electrostatics. Furthermore, we show how the local environment at the binding site affects the binding energy and propose a descriptor that serves as a predictor for the binding energy at a given site.

4.2 Introduction

Ice is one of the most widely studied substances, yet a plethora of its physicochemical properties remain poorly understood. One such property is the adsorption of water molecules on an ice surface. Deciphering the mechanisms behind this process is paramount to understanding ice growth, which plays a critical role in global climate [1,2], as well as other atmospheric phenomena [3]. Under ambient conditions ice is found in its hexagonal (Ih) phase, which is well known to have a proton disordered bulk structure. [4] The degree of proton ordering in the surface is still debated, namely due to technical limitations for experimental observations of the ice surface. The lowest energy surface is the Fletcher striped phase, where the dangling OHs are arranged in lines across the surface. [5] This surface structure was initially predicted by theoretical calculations, and later helium diffraction experiments [6] were interpreted [7] as indicating proton ordering on the surface. This interpretation was eventually brought into question [8]; however, recent novel experimental studies [9] have claimed to verify this proton ordered surface. Although this is the lowest energy surface and claims of its experimental verification have been made, it is still not widely accepted. As such, the true nature of the ice Ih surface is still in question, leaving the possibility of either ordered or disordered

surfaces. The surface structure, specifically the local environment at the binding site, will naturally play a major role in the adsorption of water molecules on the surface.

Batista and Jónsson [10] calculated binding energies of water molecules on the basal plane surface of an ice Ih crystal using the TIP4P potential. They found that 4% of the binding sites had binding energies stronger than the cohesive energy of the crystal. They further studied island formation and diffusion untangling the implications of these strong binding sites on the crystal growth. A later study reproduced their results for a proton disordered ice Ih surface, and went further by calculating the binding energy distribution for a proton ordered surface. [11] On average they found the proton ordered surface to produce smaller binding energies, however, there was still a small percentage above the cohesive energy. Thierfelder *et al.* [12] performed a follow-up study on the binding energy of water molecules on the basal surface of ice Ih using the PW91 [13] densityfunctional. Contrary to the previous findings, they did not find any binding sites with binding energies larger than the cohesive energy. Shortly after, Sun *et al.* [14] showed that the binding energy of water on the ice Ih basal surface depended on the so-called "order parameter". This order parameter is defined as,

$$C_{OH} = \frac{1}{N_{OH}} \sum_{i=1}^{N_{OH}} c_i \tag{4.1}$$

where N_{OH} is the total number of dangling OH bonds on the surface, and c_i is the number of nearest neighbor dangling OH bonds around the ith dangling OH bond. This global order parameter is a measure of the degree of ordering of the dangling OH groups on the surface of the ice. They revealed that surfaces with larger order parameters (more proton disorder) produced larger binding energies. Moreover, for surfaces with order parameters less than 2.5 no binding sites were stronger than the cohesive energy. Bringing forth the notion that the two previous studies found contradictory results simply because they used surfaces with different degrees of proton ordering. Despite these studies, the possibility of a water molecule having a binding energy larger than the cohesive energy is still contested.

Although contested, these strong binding sites have been speculated to be the cause of multiple abnormalities observed in experiments. Nordlund *et al.* [15] studied the surface of thin ice Ih films grown on Pt(111) with x-ray absorption spectroscopy, where they found an abundance of isotropically distributed dangling OHs. In particular, they found more dangling OHs than is expected for a bilayer terminated proton disordered ice Ih surface, implying a non-bilayer termination. They speculated this could be due

to water admolecules bound on these strong binding sites where annealing would not remove them from the surface. Similarly, Mehlhorn and Morgenstern [16] found that ice Ih grown on Cu(111) had no indication of a terminating bilayer at any annealing temperatures. They concluded this after observing bright spots in the STM that could not be removed by annealing, which they speculated were water admolecules at strong binding sites on the ice surface. More recently, Bockstedte *et al.* [17] used a combination of theory and experiment to show that for thin ice films grown on Cu(111) the basal surface of ice Ih was terminated by admolecule clusters. After experimentally observing a lack of a terminating bilayer, they performed DFT calculations. They found no strong binding sites for admolecules, leading them to conclude the surface must be terminated by clusters of admolecules. To better understand these experiments it is imperative that we have a comprehensive understanding of water binding on the basal surface of ice Ih.

Beyond reconciling the unexplained experimental observations, the existence of these strong binding sites would mean that ice Ih does not follow the standard growth model. A natural consequence of this is that a pristine ice surface is not possible, since annealing an admolecule at a strong binding site would result in surface melting. In order to better understand the validity of these strong binding sites, we have performed an exhaustive investigation into the binding energy of the water monomer on the basal surface of ice Ih. We employed two highly sophisticated many-body potentials, the flexible Single-Center Multipole Expansion (SCME/f) [18–21] and MB-pol [22–25], to study the adsorption of water monomers on the basal surface of ice Ih. We show that for all surfaces studied herein a site is found with binding energy larger than the cohesive energy. Furthermore, we decompose the binding energy to show the importance of dispersion in the adsorption. We also expand out the multipole contributions to the binding energy and show how quadrupole moments are significant. Finally, we show how the local environment influences the binding energy. Taking inspiration from this analysis we propose a more local "order parameter", which is more strongly correlated with the binding energy.

4.3 Methods

Orthogonal bulk cells of ice Ih containing 432 H_2O molecules with lattice parameters optimized for each potential (see Appendix) have been the starting points for constructing surface slab models. Using the ice Ih generation algorithm in the GenIce [26] program, 26 differently proton disordered 3x3x3 supercells have been created. Adding

60 Å of vacuum along the (0001) direction has then resulted in 26 pristine ice Ih(0001) surface slab models. The geometries of these slab models were optimized while keeping the atoms in the bottom half fixed at the bulk geometry positions.

For each slab, 75 random sites were selected on the surface and an H_2O admolecule was placed there and the geometry of the full system was optimized, again maintaining the bottom half of the slab fixed. The binding energies have been calculated using Equation (4.2). Consistent with previous works, the calculated binding energies have not been corrected for zero-point energies.

$$E_{BE} = E_{\text{slab}} - E_{\text{system}} \tag{4.2}$$

Contour lines for distances from dangling OHs were made by using a kernel density estimation, where Gaussians with 1.5 Å width in both dimensions were applied to each dangling OH site.

All geometry optimizations were done by first running 50 iterations of the OACCEL[27] optimizer, followed by running the conjugate gradient (CG)[28,29] method until convergence. The convergence criteria for CG geometry optimizations was always (unless stated otherwise) set to 1×10^{-5} eV/Å on the gradient norm. Lattice optimizations were done by cycling between cell optimizations with fixed scaled positions, and geometry optimizations with fixed cell vectors. Cell optimizations were run using only the CG optimizer with a convergence criteria of 1×10^{-8} eV/Å on the gradient norm. Full convergence was determined when the average change of the lattice vectors was less than 1×10^{-3} Å.

All calculations, data analysis and plotting were done using the Julia (version 1.11.6) programming language[30]. *YetAnotherSimulationSuite.jl* (YASS)[31] was used for all calculations, and it is backed by a variety of Julia packages; *Optim.jl*[32] (version 1.12.0) is used for geometry and cell optimizations, Chemfiles[33] (the *Chemfiles.jl* Julia wrapper) is used for reading and writing xyz files, and *JLD2.jl*[34] is used for storing data structures in HDF5 compliant format. Additionally, *DataFrames.jl*[35] was used during data analysis, and *Makie.jl*[36] (subpackage *CairoMakie.jl* version 0.15.4) was used for plotting. A Julia wrapper of the MBX[37] software was used to calculate MB-pol[22–25] forces and energies. Similarly, the C++ SCME/f[18–21] potential was wrapped and integrated into the Julia workflow. Proton disordered ice structures were generated using the GenIce[26] software.

4.4 Results and Discussion

We calculated the binding energy for 75 randomly selected sites across 26 surfaces with different degrees of dangling OH ordering, with C_{OH} ranging from 2 to ≈ 3.5. Figure 4.1 shows two example surfaces, one proton disordered (leftmost) and the other proton ordered (rightmost). The influence of the local environment on the binding energy can be seen within the figure. The leftmost panels show examples of a proton disordered surface, whereas the rightmost panels show a proton ordered (Fletcher-striped) surface. These plots show that although 75 sites are sampled, the results are not 75 different binding sites. This is a result of the attractive force of the dangling OHs, as can be seen by most binding sites being near dangling OHs. Sampled sites far from dangling OHs resulted in the admolecule moving to another location during the geometry optimization.

Figure 4.2 shows the binding energy distributions for each potential plotted versus the order parameter of the surface. For both potentials the distributions become broader as the order parameter increases, as expected with the increased variation in sites on the surface. In agreement with previous studies, as the order parameter increases the average binding energy for each potential also increases. Contrary to previous DFT-based studies, we find that for all surfaces studied at least one site has a binding energy larger than the cohesive energy. Across all surfaces SCME/f finds roughly 50% of sites to be one of these strong binding sites, and MB-pol finds roughly 63%.

On 25 different surfaces with order parameter of 2.0, both potentials produce at least one strong binding site (see Appendix). Moreover, for these surfaces both potentials produce an abundance of strong binding sites: for SCME/f roughly 40% of sites bind stronger than the cohesive energy and for MB-pol roughly 65%. These percentages are nearly identical to those we found for surfaces with varied order parameters, indicating a strong tendency for strong binding. Further supporting the notion that even highly ordered surfaces can produce these strong binding sites.

Additional analysis (found in the Appendix) revealed that the binding energy was strongly correlated with the induced dipole moment of the admolecule, in agreement with previous work[14]. We also find that the binding energy is closely correlated to the shortest hydrogen bond length formed between the admolecule and the surface. It is well known that DFT struggles to produce accurate descriptions of hydrogen bonds[38,39], which at first glance may seem to explain the discrepancy between our results and previous DFT-based results. However, PBE is reported to overbind hydro-

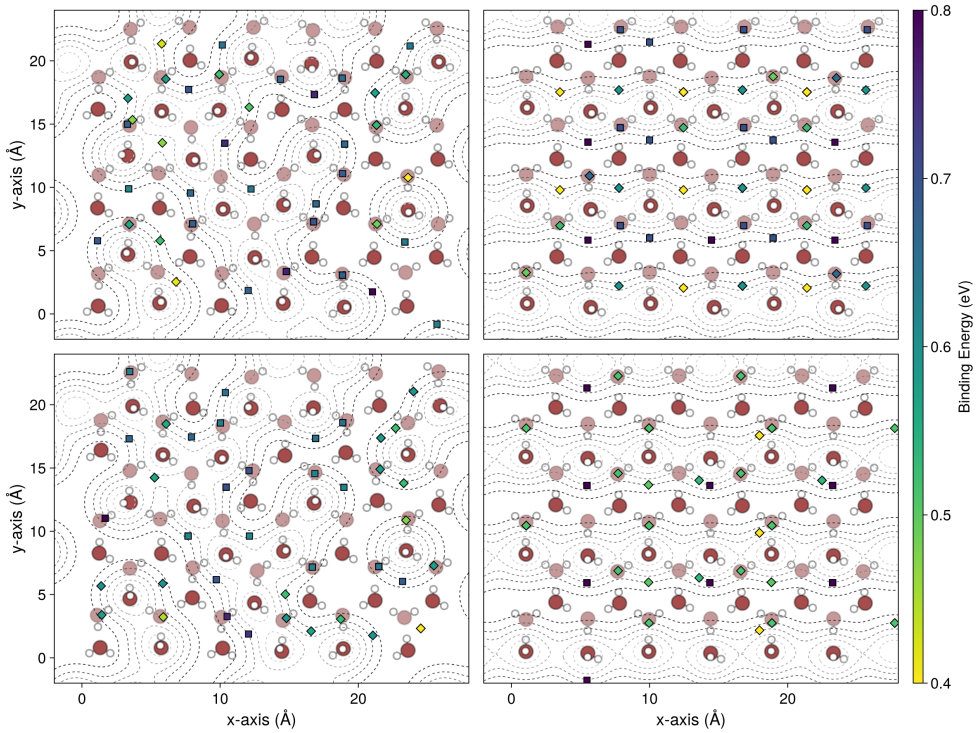

Figure 4.1: A visualization of the influence of the local environment on the binding energy. The surface bilayer is shown in reduced opacity, where red is oxygen atoms, white are hydrogen atoms. The lower layer of the bilayer is less opaque than the upper layer. The contour lines represent distance from a dangling OH, where lighter dashed lines are closer and darker dashed lines farther away from dangling OHs. The scatter points are binding sites, where the color corresponds to the binding energy for that site (as shown by the colorscale) and the marker denotes if the binding energy is above (rectangle) or below (diamond) the cohesive energy of ice Ih for the respective potential. The top panels are calculated with MB-pol and the lower panels with SCME/f. The leftmost panels are disordered surfaces, and the rightmost panels are Fletcher-striped surfaces.

gen bonds when compared to CCSD(T)[40], which both potentials are fitted to. This raises the question of what could be causing this discrepancy.

To analyze the adsorption energies in more detail we decomposed the binding energy into its constituent components within each potential. The top panels of Figure 4.3 shows the binding energies from both potentials decomposed into their constituent energy contributions. Both potentials exhibit similar decomposed contributions, namely, the electrostatic and dispersion terms have averages in very close agreement. As expected, the electrostatic contribution is the largest contribution to

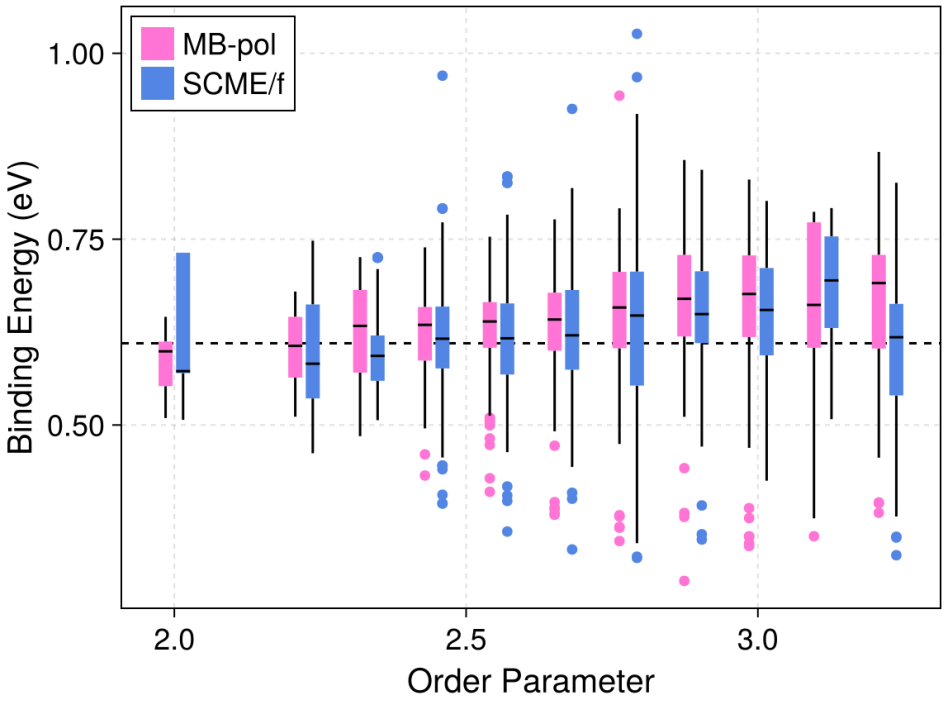

Figure 4.2: Binding energy plotted as a function of the order parameter (C_{OH}) defined in Equation (4.1). For visual clarity, MB-pol and SCME/f have artificial offsets in the x-axis. All 1950 binding sites for each potential are included. The black dashed line is the experimental cohesive energy (0.609 eV), which is close to the cohesive energy produced by MB-pol (0.608 eV) and SCME/f (0.611 eV).

the binding energy. The second largest positive contribution in both potentials is dispersion, with a contribution nearly half as large as the electrostatic contribution.

The electrostatics in both potentials can be further decomposed into multipole contributions, of which there is notably more terms included within SCME/f than in MB-pol. As such, we have decomposed the multi-pole contributions to the binding energy for SCME/f only. The bottom panel of Figure 4.3 shows the contribution of dipole, quadrupole, octupole and hexadecapole terms to the electrostatic component of the binding energy for SCME/f. As expected, the dipole term is the largest and higher order terms contribute less as the order increases. Interestingly, the quadrupole term has an average energy contribution close to that of the dipole term. This shows that for adsorption both dipole and quadrupole moments play a significant role in the energetics.

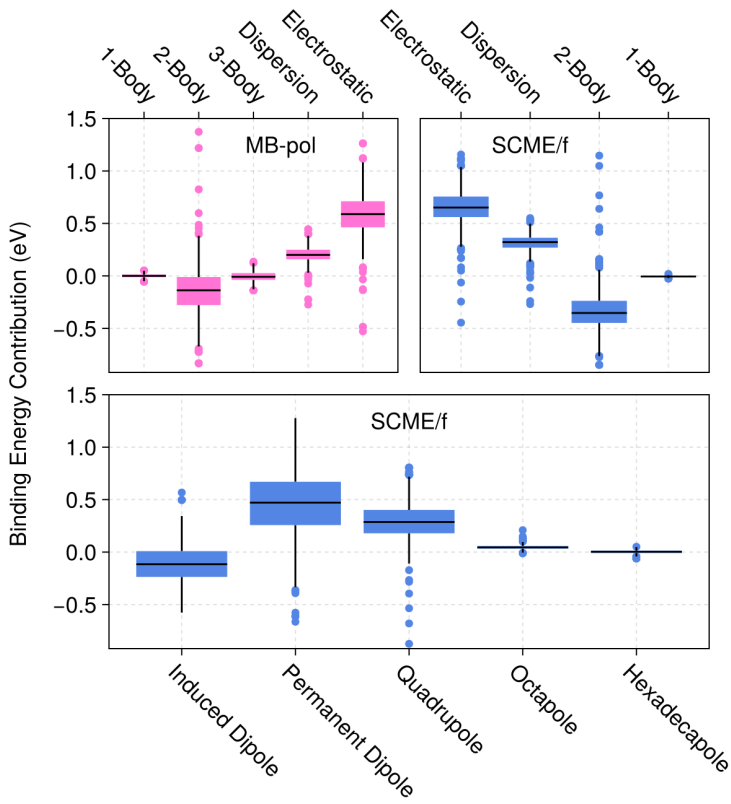

Figure 4.3: Top panels: decomposed binding energy contributions for each potential. All 1950 binding sites for each potential are included. Bottom panel: decomposed electrostatic energy contributions to the binding energy using SCME/f. All 1950 binding sites for each potential are included.

A key feature of the binding highlighted by Figure 4.1 is the importance of the alignment of the dangling OH with the oxygen atom of the admolecule. In particular, the strongest binding sites are those where the H-bond formed by the dangling OH and the admolecule is closest to being linear. This is corroborated by the trend observed between the shortest H-bond and binding energy, namely because a linear H-bond will be a shorter H-bond. For instance, looking at A-type sites in the top right panel of Figure 4.1 the energies alternate between 0.63 eV and 0.61 eV. The key difference between these sites is the direction of the in-surface H-bond formed by the molecule with the dangling OH near the binding site. The direction of this H-bond dictates how well the water molecule can align its dangling OH with the oxygen atom of the

admolecule. Rotations around the H-bond axis allow the dangling OH to pivot toward the admolecule, as such, the weakest A-type sites are those where the H-bond points away from the binding site. These sites prevent rotations that align the dangling OH, in order to compensate for this these sites result in larger H−O−H bond angles for the molecule with the dangling OH. However, limitations on the bond angle prevent the dangling OH from making an ideal alignment, resulting in smaller binding energies. This effect is more pronounced in MB-pol, where the H−O−H bond angle flexibility due to environment is larger (see Appendix). Moreover, the change in the H−O−H bond angle for molecules with dangling OHs near a binding site before and after binding is larger for MB-pol than SCME/f (see Appendix). This bond angle flexibility in MB-pol causes the binding energy distributions to be narrower than those calculated with SCME/f.

Although the binding energy is correlated in some ways to the order parameter, there is still a large variation in binding sites per order parameter (see Figure 4.2). This is due to the order parameter being insensitive to the local environment at the adsorption site, which plays the dominant role in the binding energy (see Figure 4.1). Drawing inspiration from the analysis we have done, we have constructed a "local environment parameter",

$$C = \sum_{i}^{NN} \frac{\pi - (0.5\pi - \theta_i)^3}{r_i^3} + \sum_{i}^{N} \frac{1}{r_i^3} \tag{4.3}$$

where NN is the number of dangling OHs within 4 Å from the adsorption site, N is the number of dangling OHs further than 4 Å from the adsorption site, r is the distance from the dangling OH, and θ is the angle formed between the site, dangling OH, and the additional hydrogen atom on the surface molecule with the dangling OH. The angle is used to account for how rotations around the H-bond axis allow for the dangling OH to better align with the admolecule.

Figure 4.4 shows the binding energies as a function of the local environment parameter using both potentials, separately for both A-type and B-type adsorption sites. A clear trend is observed where increasing the local environment parameter increases the binding energy. This gives a more robust predictor of how what the binding energy for a site on a surface will be.

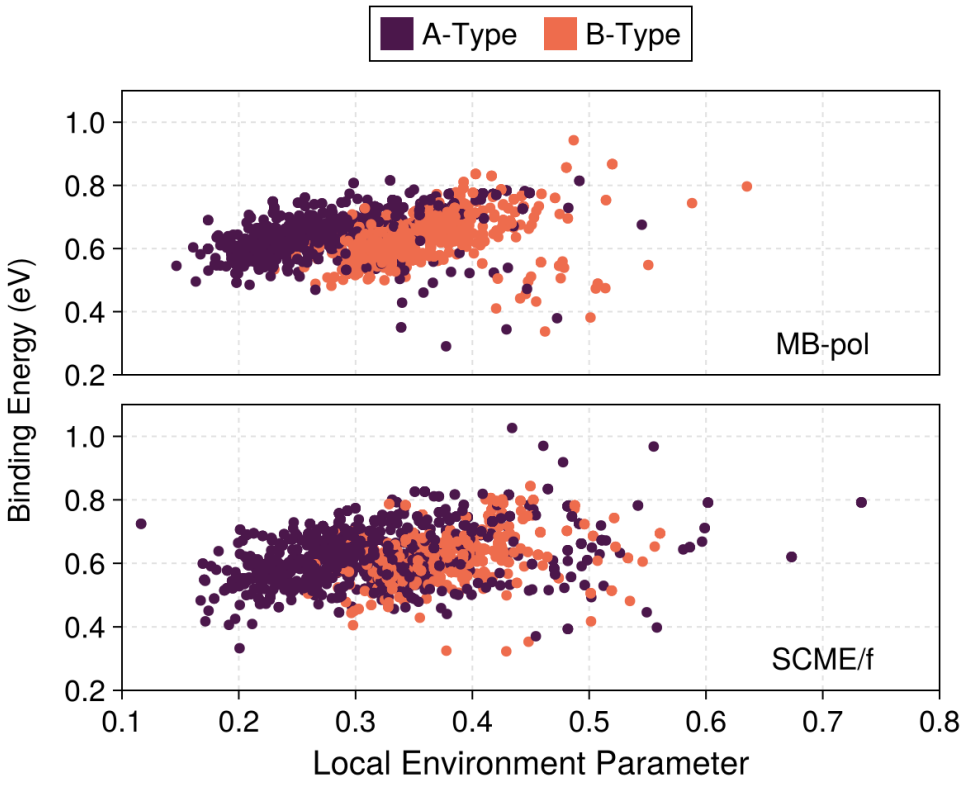

Figure 4.4: Binding energy as a function of the local environment parameter.

4.5 Conclusion

We have done an exhaustive analysis of the physicochemical properties involved in the adsorption of water monomers on the basal surface of ice Ih. Utilizing highly sophisticated potentials we have shown that binding sites with energies larger than the cohesive energy can be found on surfaces with any degree of proton ordering. We have also revealed that the dominant term in the binding is the electrostatic term, where the dipole and quadrupole terms are significant contributors to the binding energy. Additionally, we show that dispersive interactions also contribute significantly to the adsorption process. Furthermore, we show that the local environment is crucial to the binding, and cannot be simply reduced down to distances from dangling OHs or degree of surface ordering. Finally, we have constructed a local environment parameter

which serves as an improved descriptor for how slab structure will influence binding energies.

Our results have significant implications for ice surface growth, meaning that a pristine ice Ih surface is not possible. This has implications for various atmospheric phenomena, which are vital to global climate studies. Furthermore, the confirmation of the existence of these strong binding sites helps shine light on many unexplained experimental observations, specifically those that observed a non-bilayer-terminated ice surface.

4.A Appendix

4.A.1 Optimized Lattice Vectors and Cohesive Energy

Table 4.A.1 compiles the optimized lattice vectors and cohesive energies of the bulk phase ice Ih structures calculated by each potential.

Table 4.A.1: Lattice parameters a and c (Å) and cohesive energies (meV) of bulk ice Ih, calculated for each potential.

Potential	a	c	E_{coh}
Expt [41,42]	8.98	7.33	-609
MB-pol	8.935	7.284	-607.5
SCME/f	8.889	7.239	-611.4

4.A.2 Order Paremeter 2.0 Surfaces

Figure 4.A.5 shows the binding energy distributions with both potentials for 25 surfaces with order parameter 2. This set of 25 surfaces contains Fletcher striped surfaces and glide surfaces, both of which have order parameter 2.

4.A.3 Binding Energy Correlations

Figure 4.A.6 shows the correlation between the induced dipole moment of the admolecule and the binding energy. This contains all data from all binding sites across all surfaces studied herein.

Figure 4.A.7 shows the correlation between the shortest hydrogen bond formed between the admolecule and the surface and the binding energy. This also contains all data from all binding sites across all surfaces studied herein.

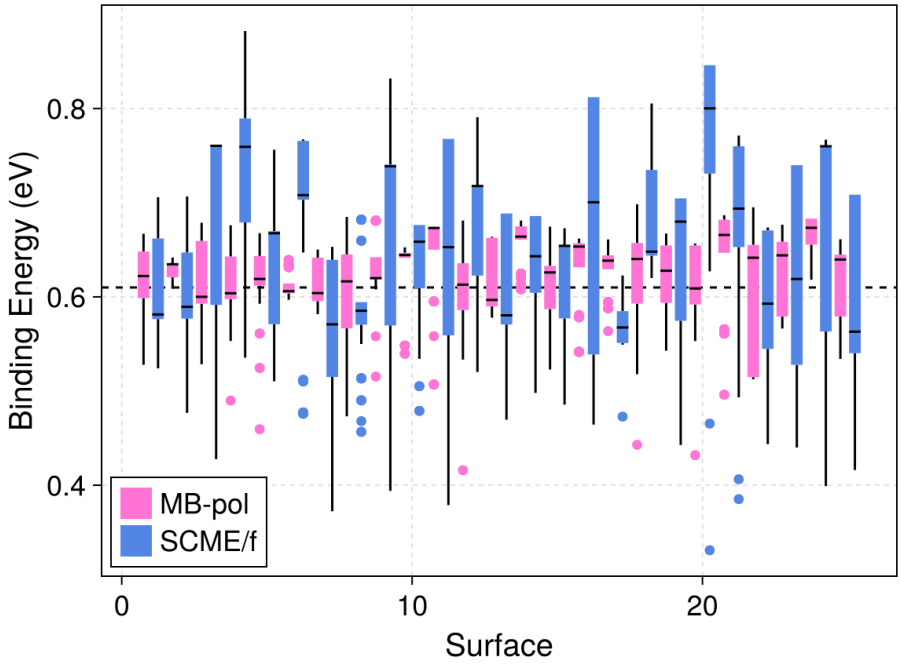

Figure 4.A.5: Binding energy distributions for surfaces with order parameter 2.

4.A.4 Bond Angle Analysis

Figure 4.A.8 shows the distribution of water bond angles for molecules within the bulk and surface bilayer using both potentials. This contains data from all slabs used herein.

Figure 4.A.9 shows the distribution of the difference between the water bond angle of a molecule with a dangling OH before and after binding. This contains data from all slabs used herein.

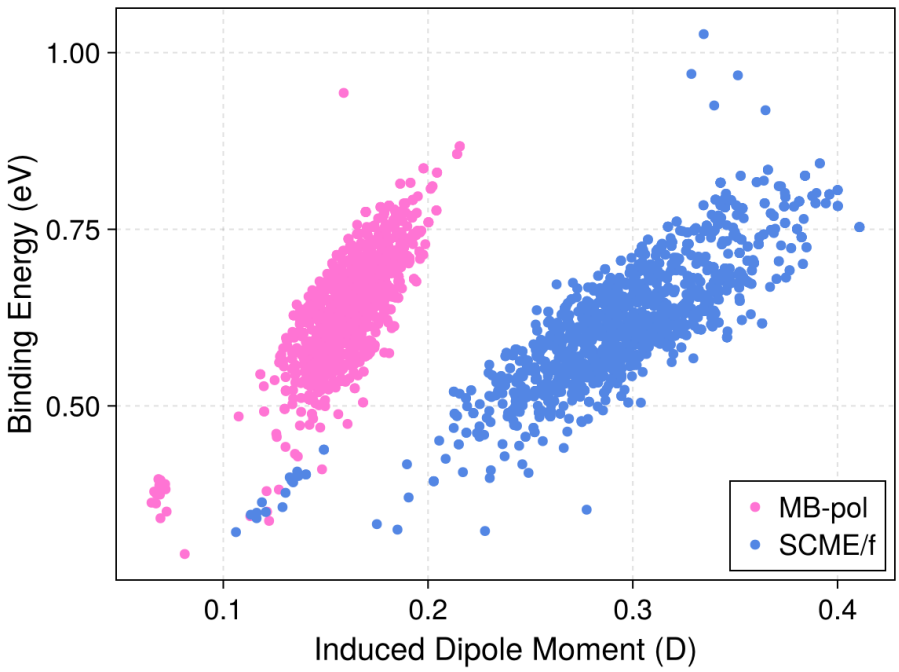

Figure 4.A.6: Binding energy versus the induced dipole moment of the admolecule.

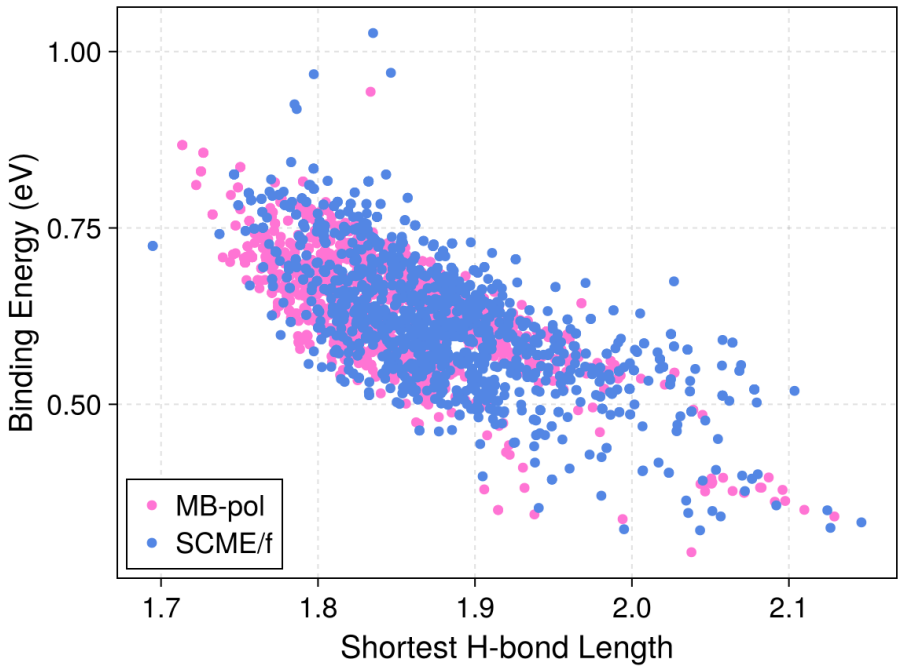

Figure 4.A.7: Binding energy versus shortest hydrogen bond formed between the adsorbate molecule and the surface.

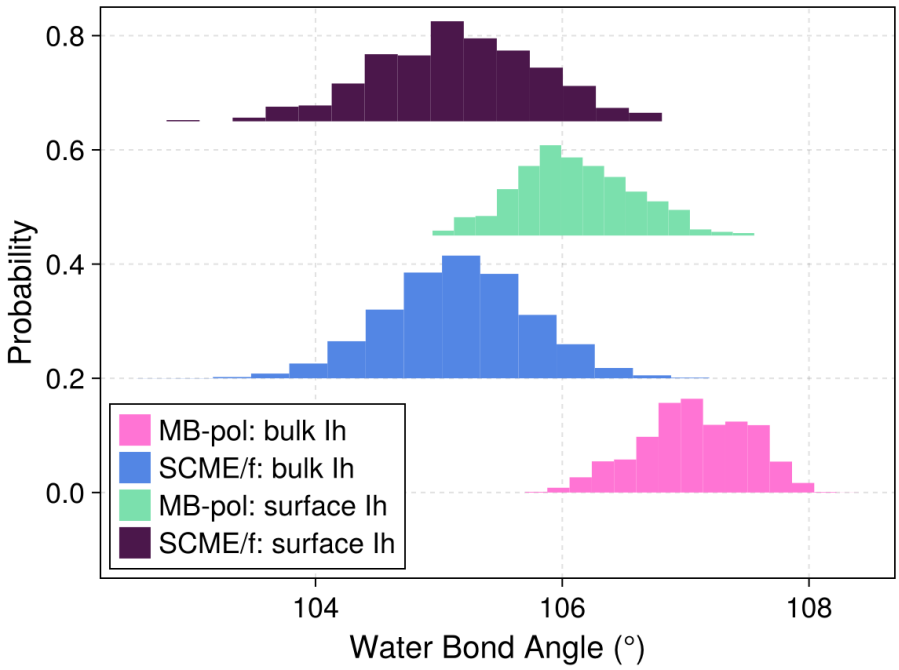

Figure 4.A.8: The distribution of water bond angles for bulk phase structures, and surface bilayer molecules in slab structures with MB-pol and SCME/f.

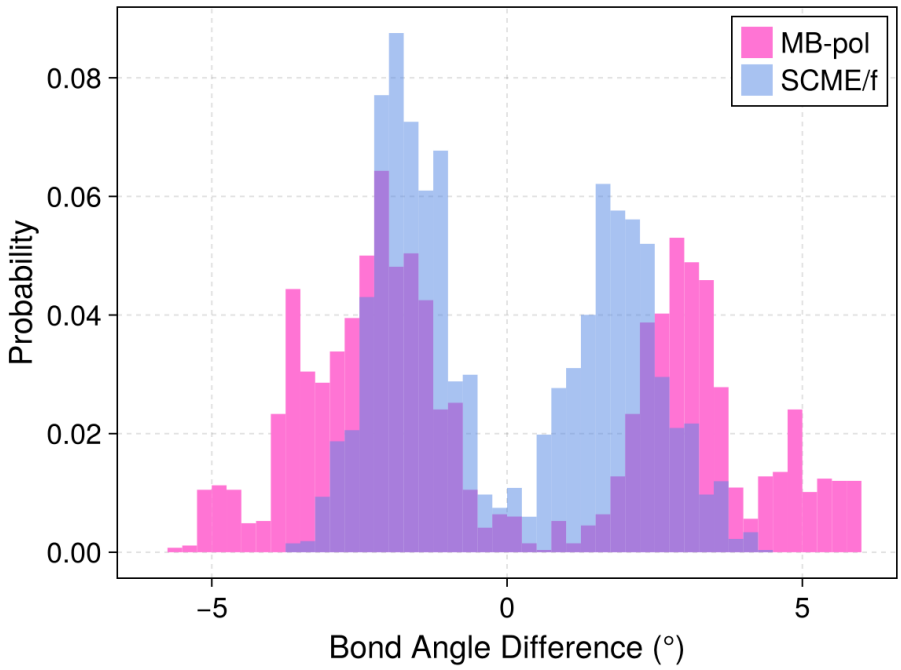

Figure 4.A.9: The difference in the H−O−H bond anlge of the water molecules with dangling OHs near binding sites before and after binding.

4.B Bibliography

[1] Petr G Sennikov, Stanislav K Ignatov, and Otto Schrems. Complexes and clusters of water relevant to atmospheric chemistry: H2o complexes with oxidants. *ChemPhysChem*, 6(3):392–412, 2005.

[2] Trude Storelvmo. Aerosol effects on climate via mixed-phase and ice clouds. *Annual Review of Earth and Planetary Sciences*, 45(1):199–222, 2017.

[3] Jonathan PD Abbatt. Interactions of atmospheric trace gases with ice surfaces: Adsorption and reaction. *Chemical Reviews*, 103(12):4783–4800, 2003.

[4] Victor F Petrenko and Robert W Whitworth. *Physics of ice*. OUP Oxford, 1999.

[5] Neville H Fletcher. Reconstruction of ice crystal surfaces at low temperatures. *Philosophical Magazine B*, 66(1):109–115, 1992.

[6] A Glebov, AP Graham, A Menzel, JP Toennies, and P Senet. A helium atom scattering study of the structure and phonon dynamics of the ice surface. *The Journal of Chemical Physics*, 112(24):11011–11022, 2000.

[7] V Buch, H Groenzin, I Li, MJ Shultz, and E Tosatti. Proton order in the ice crystal surface. *Proceedings of the National Academy of Sciences*, 105(16):5969–5974, 2008.

[8] N Avidor and W Allison. Helium diffraction as a probe of structure and proton order on model ice surfaces. *The Journal of Physical Chemistry Letters*, 7(22): 4520–4523, 2016.

[9] Yuki Nojima, Yudai Suzuki, Misato Takahashi, and Shoichi Yamaguchi. Proton order toward the surface of ice ih revealed by heterodyne-detected sum frequency generation spectroscopy. *The Journal of Physical Chemistry Letters*, 8(20):5031–5034, 2017.

[10] Enrique R Batista and Hannes Jónsson. Diffusion and island formation on the ice ih basal plane surface. *Computational Materials Science*, 20(3-4):325–336, 2001.

[11] Andreas Pedersen, Leendertjan Karssemeijer, Herma M Cuppen, and Hannes Jónsson. Long-time-scale simulations of h2o admolecule diffusion on ice ih (0001) surfaces. *The Journal of Physical Chemistry C*, 119(29):16528–16536, 2015.

[12] C Thierfelder, A Hermann, P Schwerdtfeger, and WG Schmidt. Strongly bonded water monomers on the ice ih basal plane: Density-functional calculations. *Physical Review B—Condensed Matter and Materials Physics*, 74(4):045422, 2006.

[13] John P Perdew and Yue Wang. Accurate and simple analytic representation of the electron-gas correlation energy. *Physical Review B*, 45(23):13244, 1992.

[14] Zhaoru Sun, Ding Pan, Limei Xu, and Enge Wang. Role of proton ordering in adsorption preference of polar molecule on ice surface. *Proceedings of the National Academy of Sciences*, 109(33):13177–13181, 2012.

[15] D Nordlund, H Ogasawara, Ph Wernet, M Nyberg, M Odelius, LGM Pettersson, and A Nilsson. Surface structure of thin ice films. *Chemical Physics Letters*, 395 (1-3):161–165, 2004.

[16] Michael Mehlhorn and Karina Morgenstern. Faceting during the transformation of amorphous to crystalline ice. *Physical Review Letters*, 99(24):246101, 2007.

[17] Michel Bockstedte, Anja Michl, Manuel Kolb, Michael Mehlhorn, and Karina Morgenstern. Incomplete bilayer termination of the ice (0001) surface. *The Journal of Physical Chemistry C*, 120(2):1097–1109, 2016.

[18] Enrique Ricardo Batista. *Development of a new water-water interaction potential and application to molecular processes in ice*. University of Washington, 1999.

[19] Kjartan Thor Wikfeldt, ER Batista, FD Vila, and H Jónsson. A transferable h 2 o interaction potential based on a single center multipole expansion: Scme. *Physical Chemistry Chemical Physics*, 15(39):16542–16556, 2013.

[20] Elvar Orn Jonsson, Asmus Ougaard Dohn, and Hannes Jonsson. Polarizable embedding with a transferable h2o potential function i: Formulation and tests on dimer. *Journal of Chemical Theory and Computation*, 15(12):6562–6577, 2019.

[21] Elvar Orn Jonsson, Soroush Rasti, Marta Galynska, Jorg Meyer, and Hannes Jónsson. Transferable potential function for flexible h2o molecules based on the single-center multipole expansion. *Journal of Chemical Theory and Computation*, 18(12):7528–7543, 2022.

[22] Volodymyr Babin, Claude Leforestier, and Francesco Paesani. Development of a "first principles" water potential with flexible monomers: Dimer potential energy surface, vrt spectrum, and second virial coefficient. *Journal of Chemical Theory and Computation*, 9(12):5395–5403, 2013.

[23] Volodymyr Babin, Gregory R Medders, and Francesco Paesani. Development of a "first principles" water potential with flexible monomers. ii: Trimer potential energy surface, third virial coefficient, and small clusters. *Journal of Chemical Theory and Computation*, 10(4):1599–1607, 2014.

[24] Gregory R Medders, Volodymyr Babin, and Francesco Paesani. Development of a "first-principles" water potential with flexible monomers. iii. liquid phase properties. *Journal of Chemical Theory and Computation*, 10(8):2906–2910, 2014.

[25] Francesco Paesani. Getting the right answers for the right reasons: Toward predictive molecular simulations of water with many-body potential energy functions. *Accounts of Chemical Research*, 49(9):1844–1851, 2016.

[26] Masakazu Matsumoto, Takuma Yagasaki, and Hideki Tanaka. Genice: hydrogen-disordered ice generator, 2018.

[27] Asbjørn Nilsen Riseth. Objective acceleration for unconstrained optimization. *Numerical Linear Algebra with Applications*, 26(1):e2216, 2019.

[28] William W Hager and Hongchao Zhang. Algorithm 851: Cg_descent, a conjugate gradient method with guaranteed descent. *ACM Transactions on Mathematical Software (TOMS)*, 32(1):113–137, 2006.

[29] William W Hager and Hongchao Zhang. The limited memory conjugate gradient method. *SIAM Journal on Optimization*, 23(4):2150–2168, 2013.

[30] Jeff Bezanson, Alan Edelman, Stefan Karpinski, and Viral B Shah. Julia: A fresh approach to numerical computing. *SIAM Review*, 59(1):65–98, 2017.

[31] Brian C Ferrari. YetAnotherSimulationSuite.jl: An atomic simulation suite in julia. *Journal of Open Source Software*, 10(116):9480, 2025.

[32] P Mogensen and A Riseth. Optim: A mathematical optimization package for julia. *Journal of Open Source Software*, 3(24):615, 2018.

[33] Guillaume Fraux, Jonathan Fine, ezavod, German P. Barletta, Laura Scalfi, and Mykola Dimura. chemfiles/chemfiles: Version 0.9.3, February 2020. URL `https://doi.org/10.5281/zenodo.3653157`.

[34] Jonas Isensee. Jld2.jl. `https://github.com/JuliaIO/JLD2.jl`, 2025.

[35] Milan Bouchet-Valat and Bogumił Kamiński. Dataframes. jl: Flexible and fast tabular data in julia. *Journal of Statistical Software*, 107:1–32, 2023.

[36] Simon Danisch and Julius Krumbiegel. Makie.jl: Flexible high-performance data visualization for julia. *Journal of Open Source Software*, 6(65):3349, 2021.

[37] Marc Riera, Christopher Knight, Ethan F Bull-Vulpe, Xuanyu Zhu, Henry Agnew, Daniel GA Smith, Andrew C Simmonett, and Francesco Paesani. Mbx: A many-body energy and force calculator for data-driven many-body simulations. *The Journal of Chemical Physics*, 159(5), 2023.

[38] Joel Ireta, Jörg Neugebauer, and Matthias Scheffler. On the accuracy of dft for describing hydrogen bonds: dependence on the bond directionality. *The Journal of Physical Chemistry A*, 108(26):5692–5698, 2004.

[39] A Daniel Boese. Density functional theory and hydrogen bonds: are we there yet? *ChemPhysChem*, 16(5):978–985, 2015.

[40] Michael J Gillan, Dario Alfe, and Angelos Michaelides. Perspective: How good is dft for water? *The Journal of Chemical Physics*, 144(13), 2016.

[41] Edward Whalley. Energies of the phases of ice at zero temperature and pressure. *Journal of Chemical Physics*, 81(9):4087–4092, 1984.

[42] K Röttger, A Endriss, Jörg Ihringer, S Doyle, and WF Kuhs. Lattice constants and thermal expansion of h2o and d2o ice ih between 10 and 265 k. *Acta Crystallographica*, 50(6):644–648, 1994.

4.7 Bibliography